



A new boundary element method for modeling wave propagation in functionally graded materials

Yang Yang^{*}, Yijun Liu

Department of Mechanics and Aerospace Engineering, Southern University of Science and Technology, Shenzhen, 518055, China

ARTICLE INFO

Keywords:

Wave propagation
Functionally graded material
New Green's identity
Boundary integral equation
Boundary element method

ABSTRACT

In this paper, a boundary element method (BEM) based on a new boundary integral equation (BIE) formulation is proposed for modeling wave propagation problems in functionally graded materials (FGM) in the frequency domain. The material properties of the considered FGMs are assumed to be graded along spatial Cartesian coordinates, and can vary continuously either in a single axis, or in multiple axes simultaneously, according to an exponential law distribution. Similar to the Somigliana's identity, a new generalized Green's identity corresponding to the elastodynamic equations for FGMs is established first, which can be used to derive the BIE for wave propagation in FGMs for either 2-D or 3-D models. For convenience, a special case with the static and isotropic fundamental solutions are adopted in applying the Green's identity of FGMs. Finally, a boundary-domain integral equation with boundary-only solution scheme is derived. The BEM is applied to solve the BIE and quadratic elements are employed in the discretization. Several test problems in 2-D domains are studied using the BEM. The effects of the material gradient, gradation direction, as well as frequencies of the incident wave on the wave propagation in the FGMs are investigated intensively. The numerical results clearly show the effectiveness and efficiency of the developed BEM in modeling the wave propagation problems in FGMs.

1. Introduction

Functionally graded materials (FGMs) are a type of smart composite materials which contain two or more different constituents in a designed manner. The most special characteristics of the FGMs are their material properties can change continuously in a pre-defined manner. This leads to the FGMs to have a micro-nonhomogeneous and a macro-continuous property. The outstanding properties of the FGMs have made them to have many advantages in thermal, corrosion, wear resistant, high strength with low weight, and so on. Compared with the traditional composite materials where delamination cracks often occur between different layers, FGMs offer much better crack resistance and thus have gained widespread interests in many engineering fields (Mahamood and Akinlabi, 2017).

In recent years, the research on FGMs is no longer limited to the basic static stress analysis. It has also been extended into other application fields. For example, FGMs have been used to design the coating to absorb the acoustic wave propagation; FGM multimode optical fibers have been used in communication fields, and FGM piezoelectric sensors have been developed with wide applications (Fengxiang et al., 2018).

Research on the wave propagation in FGMs has also been conducted. A 1-D model for designing FGMs to manage stress waves was proposed by Bruck (2000). This model was initially applied to FGMs with discrete layering, then extended to continuously graded architectures. Berezovski et al. (2003) studied the propagation of stress wave propagation in FGMs numerically by means of the composite wave-propagation algorithm. Two distinct models of FGMs were considered, one was a multilayered metal-ceramic composite with averaged properties with layers, the other was randomly embedded ceramic particles in a metal matrix with prescribed volume fraction. A new higher-order spectral element was developed by Chakraborty et al. (Chakraborty and Gopalakrishnan, 2004) for wave propagation analysis of an FGM beam in the presence of the thermal and mechanical loading. The Young's modulus and thermal expansion varied on the beam depth. Aksoy and Senocak (2009) analyzed the wave propagation in functionally graded and layered materials by using space-time discontinuous Galerkin method. The wave propagation and dynamic response of the rectangular FGM plates with completed clamped supports under impulse load were analyzed by Sun and Luo (2011). The effective material properties of FGMs for the plate were assumed to vary continuously through the plate

^{*} Corresponding author.

E-mail address: yangy33@sustech.edu.cn (Y. Yang).

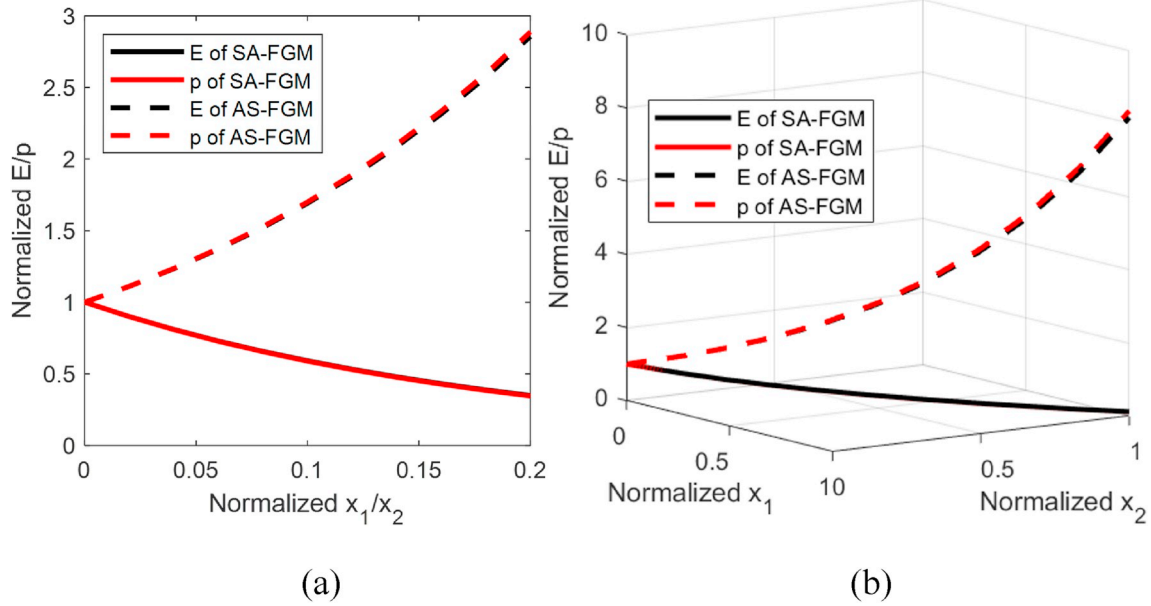


Fig. 1. Material properties varying along special coordinates: (a) in x_1 or x_2 coordinate respectively; (b) in x_1 and x_2 simultaneously.

thickness and be distributed according to a volume fraction power law along the plate thickness. Numerical modeling of the lamb wave propagation in FGMs by a 2-D time-domain spectral finite element method (SpFEM) was presented by Hedayatrasa et al. (2014). The high-order Chebyshev polynomials as approximation functions were used, which provided the capability to take into account the through thickness variation of the material properties. Elastic wave propagation in FG circular cylinders were discretized by Dorduncu et al. (2015) by using the finite difference method. The cylinder material consists of metal and ceramic, and material properties varied through the thickness direction with a power-law distribution in terms of volume fractions of the constituents. A new model for wave propagation in FG anisotropic doubly-curved shells was devoted by Aminipour et al. (2018) in the framework of an accurate higher-order shear deformation theory. An exponential formula in combination with a trigonometric function were used for modeling the displacement field. All components of the elastic stiffness tensor and density were varied exponentially through the thickness direction. The one-dimensional propagation of longitudinal elastic waves along the thickness of a plate made of FGMs excited by a harmonic force was reported by Benarik et al. (Bednarik et al., 2018). The material properties of the plate were assumed smoothly connects the material properties of the upper and lower homogeneous materials that bounds the plate. The Incy-type equation was transformed to Heun's equation a local exact solution of which was expressed in terms of local Heun functions. The study presented an improved mathematical model to analyze the stress wave propagation in adhesively bonded FG circular cylinders (butt joint) under an axial impulsive load was proposed by Dorduncu (Dorduncu et al., 2019). The volume fractions of the material constituents in the upper and lower cylinders were functionally tailored through the thickness of each cylinder using a power-law. In this improved model, the governing equations of the wave propagation include the spatial derivatives of local mechanical properties and were discretized by means of the finite difference method. An analysis of the propagation of wave FG plates was presented by Fourn et al. (2018) by using a high order hyperbolic shear deformation theory. Because the shear correction coefficient is not required, the theory has only four variables. The governing equations of the wave propagation in the FG plate were derived by employing the Hamilton's principle.

Due to the material inhomogeneity, a new challenge presents in the analysis of the wave propagation in FGMs. The traditional definition of the plane wave is no longer valid and the waves in such medium

propagate with attenuation. The literature of wave propagation in nonhomogeneous materials is vast as shown in the above paragraph, where the waves are successfully described by wave modes, and their dispersive character. The propagation speed, attenuation constant, and pertinent angles are in general dependent on the frequency (Gopalakrishnan, 2016). However, most of the work covered the wave propagation problems in time domain. Meanwhile, the material properties investigated only vary in the thickness direction of the considered thin structures, with limited understanding of the physical behavior of the wave propagation in the inhomogeneous materials and in frequency domain. In the present work, the wave propagation in an FGM media is studied in the frequency domain, and the material properties vary along the spatial coordinates either in a single direction, or in multiple directions simultaneously, according to an exponential law distribution. The boundary integral equation (BIE) for frequency domain wave propagation in FGMs is developed by deriving a new generalized Green's identity corresponding to the elastodynamic equations for FGMs. The boundary element method (BEM) is then applied to solve the BIE.

This paper is organized as follows: In Section 2, the distribution of material properties for considered FGM is presented. In Section 3, a new Green's identity and the BIE for wave propagation problems in the FGM are derived. In Section 4, the accuracy and the efficiency of the present method is verified by solving the wave propagation in homogeneous and FGM materials. In Section 5, the present method is applied to investigate the physical behaviors of wave propagation in several FGMs, and detail parametric study is conducted. The paper concludes with a summary in Section 6.

2. Material properties of the FGM

In this paper, a two-material FGM is considered in the 2-D case. An exponential law is used to simulate the Young's modulus E and mass density ρ for the FGM as follows:

$$E = E_s e^{(\beta x_1 + \gamma x_2)}, \quad \text{where} \quad \beta = \frac{1}{L_1} \ln\left(\frac{E_c}{E_s}\right), \quad \gamma = \frac{1}{L_2} \ln\left(\frac{E_c}{E_s}\right), \quad (1a)$$

$$\rho = \rho_s e^{(\xi x_1 + \eta x_2)}, \quad \text{where} \quad \xi = \frac{1}{L_1} \ln\left(\frac{\rho_c}{\rho_s}\right), \quad \eta = \frac{1}{L_2} \ln\left(\frac{\rho_c}{\rho_s}\right), \quad (1b)$$

where x_1, x_2 represent the Cartesian coordinates, respectively. L_1 and L_2

describe the length and height of the considered geometry in Cartesian coordinate. E_s, E_e, ρ_s, ρ_e are the Young's modulus and mass density for the starting and ending face respectively. β, γ, ξ, η indicate the material gradation parameters. The material properties of the FGM can vary from pure steel to pure aluminum and vice versa along x_1 ($\gamma = 0, \eta = 0$) or x_2 ($\beta = 0, \xi = 0$), respectively or simultaneously ($\beta, \gamma, \xi, \eta \neq 0$). Taking a metal/aluminum FGM as an example, the material properties varying along the spatial Cartesian coordinates are depicted in Fig. 1, where the material starting from steel and varying gradually to aluminum is denoted as SA, and conversely, the material varying gradually from aluminum to steel is denoted as AS.

3. Boundary integral equation formulations

A new generalized Green's identity is derived first, that will be employed to establish the BIE for FGM wave propagation problems. Assume that the considered domain Ω has two states, and each state has a different type of functionally graded material. The Young's modulus, Poisson's ratio and mass density for these two FGMs are denoted by E, ν, ρ and E^*, ν^*, ρ^* , respectively. The frequency domain wave propagation equilibrium and constitutive equations for these two states are listed below:

$$\left. \begin{aligned} \text{Equilibrium : } & \sigma_{ij,j} + \omega^2 \rho u_i = 0 \\ \text{Constitutive : } & \sigma_{ij} = \mu(\mathbf{x}) c_{ijkl} u_{k,l} \end{aligned} \right\} \text{ for FGM 1 } \left(E, \nu, \rho \right), \quad (2a, b)$$

$$\left. \begin{aligned} \text{Equilibrium : } & \sigma_{ij,j}^* + \omega^2 \rho^* u_i^* = 0 \\ \text{Constitutive : } & \sigma_{ij}^* = \mu^*(\mathbf{x}) c_{ijkl}^* u_{k,l}^* \end{aligned} \right\} \text{ for FGM 2 } \left(E^*, \nu^*, \rho^* \right), \quad (3a, b)$$

where ω indicates the circular frequency of the incident wave. The tensors $\sigma_{ij}, \sigma_{ij}^*$ and vectors u_i, u_i^* are the stress and displacement components, respectively, for the two states. Functions $\mu(\mathbf{x})$ and $\mu^*(\mathbf{x})$ are the shear modulus of the FGMs which vary continuously along certain special coordinates. The scaled Young's modulus tensors are $c_{ijkl} = \frac{2\nu}{1-2\nu} \delta_{ij} \delta_{kl} + \delta_{ik} \delta_{jl} + \delta_{il} \delta_{jk}$ and $c_{ijkl}^* = \frac{2\nu^*}{1-2\nu^*} \delta_{ij} \delta_{kl} + \delta_{ik} \delta_{jl} + \delta_{il} \delta_{jk}$, where ν and ν^* are both assumed to be constant.

This new Green's identity can be derived by using the Gauss theorem as follows. First, evaluate the integral:

$$\begin{aligned} \int_{\Omega} \sigma_{ij,j} u_i^* d\Omega &= \int_{\Omega} (\sigma_{ij} u_i^*)_{,j} d\Omega - \int_{\Omega} \sigma_{ij} u_{i,j}^* d\Omega = \int_{\Gamma} (\sigma_{ij} u_i^*) n_j d\Gamma - \int_{\Omega} \sigma_{ij} u_{i,j}^* d\Omega \\ &= \int_{\Gamma} t_i u_i^* d\Gamma - \int_{\Omega} \sigma_{ij} u_{i,j}^* d\Omega = \int_{\Gamma} t_i u_i^* d\Gamma - I \end{aligned} \quad (4)$$

where n_j is the component of the outward unit normal n to the boundary Γ of the considered domain Ω , and the last term I in Eq. (4) is defined as:

$$I \equiv \int_{\Omega} \sigma_{ij} u_{i,j}^* d\Omega = \int_{\Omega} [\mu(\mathbf{x}) c_{ijkl} u_{k,l}] u_{i,j}^* d\Omega. \quad (5)$$

If we assume $\nu = \nu^*$, then $c_{ijkl} = c_{ijkl}^*$. Thus, I in Eq. (5) can be evaluated as:

$$\begin{aligned} I &\equiv \int_{\Omega} \sigma_{ij} u_{i,j}^* d\Omega = \int_{\Omega} [\mu(\mathbf{x}) c_{ijkl} u_{k,l}] u_{i,j}^* d\Omega = \int_{\Omega} \mu(\mathbf{x}) [c_{ijkl}^* u_{k,l}^*] u_{i,j}^* d\Omega \\ &= \int_{\Omega} \kappa(\mathbf{x}) [\mu^*(\mathbf{x}) c_{klj}^* u_{i,j}^*] u_{k,l}^* d\Omega = \int_{\Omega} \kappa(\mathbf{x}) \sigma_{kl}^* u_{k,l}^* d\Omega = \int_{\Omega} \kappa(\mathbf{x}) \sigma_{ij}^* u_{i,j}^* d\Omega \\ &= \int_{\Omega} [\kappa(\mathbf{x}) \sigma_{ij}^* u_i]_{,j} d\Omega - \int_{\Omega} [\kappa(\mathbf{x}) \sigma_{ij}^*]_{,j} u_i d\Omega \\ &= \int_{\Gamma} [\kappa(\mathbf{x}) \sigma_{ij}^* u_i] n_j d\Gamma - \int_{\Omega} [\kappa(\mathbf{x}) \sigma_{ij}^*]_{,j} u_i d\Omega \\ &= \int_{\Gamma} \kappa(\mathbf{x}) t_i^* u_i d\Gamma - \int_{\Omega} [\kappa(\mathbf{x}) \sigma_{ij}^*]_{,j} u_i d\Omega \end{aligned} \quad (6)$$

in which $\kappa(\mathbf{x}) = \frac{\mu(\mathbf{x})}{\mu^*(\mathbf{x})}$. Then, substituting Eq. (6) into Eq. (4), the generalized Green's identity for the FGM problem can be written as:

$$\int_{\Omega} \sigma_{ij,j} u_i^* d\Omega - \int_{\Omega} [\kappa(\mathbf{x}) \sigma_{ij}^*]_{,j} u_i d\Omega = \int_{\Gamma} t_i u_i^* d\Gamma - \int_{\Gamma} \kappa(\mathbf{x}) t_i^* u_i d\Gamma, \quad (7)$$

which is similar to the Somigliana's identity for elastostatic problems (Liu, 2009). Eq. (7) is the generalized Green's identity for the FGM problems, which can be used to analyze elastodynamic problems of FGMs for either 2-D or 3-D models. However, at the present, the fundamental solution for FGMs are either not available or too complicated (Gao and Davies, 2011), which prohibits efficient numerical implementation and extension of the BEM to solving the dynamic FGM problems. To circumvent this difficulty, a special case of using the static and isotropic fundamental solution will be adopted in applying Eq. (7) for solving dynamic FGM problems.

First, we take $\mu^*(\mathbf{x}) = \mu_0$, where μ_0 represents the shear modulus of the isotropic and homogenous material, then $\kappa(\mathbf{x}) = \frac{\mu(\mathbf{x})}{\mu_0}$ and identity in Eq. (7) becomes:

$$\int_{\Omega} \sigma_{ij,j} u_i^* d\Omega - \int_{\Omega} \kappa(\mathbf{x}) \sigma_{ij,j}^* u_i d\Omega = \int_{\Gamma} t_i u_i^* d\Gamma - \int_{\Gamma} \kappa(\mathbf{x}) t_i^* u_i d\Gamma + \int_{\Omega} \kappa(\mathbf{x})_{,j} \sigma_{ij}^* u_i d\Omega. \quad (8)$$

In Eq. (8), let u_i, t_i, σ_{ij} be the solution of the boundary-value problem that needs to be solved for the given FGM case, and $u_i^*, t_i^*, \sigma_{ij}^*$ be the fundamental solutions of the static linear elastic homogeneous material with shear modulus equal to 1. For 2-D, one has:

$$u_i^* = U_{ij} = \frac{-1}{8\pi(1-\nu)} [(3-4\nu)\delta_{ij} \ln(r) - r_i r_j], \quad (9)$$

$$t_i^* = T_{ij} = \frac{-1}{4\pi(1-\nu)r} [(1-2\nu)(n_i r_j - n_j r_i) + ((1-2\nu)\delta_{ij} + 2r_i r_j) r_i n_j], \quad (10)$$

$$\sigma_{ijk}^* = \Sigma_{ijk,k}(\mathbf{x}, \mathbf{y}), \text{ where } \Sigma_{ijk,k}(\mathbf{x}, \mathbf{y}) + \delta_{ij} \delta(\mathbf{x}, \mathbf{y}) = 0, \quad \forall \mathbf{x}, \mathbf{y} \in R^2/R^3 \quad (11)$$

where $(\cdot)_{,k} = \partial(\cdot)/\partial y_k$, and $r = |\mathbf{x}-\mathbf{y}|$, is the distance between the source point \mathbf{x} and the field point \mathbf{y} . The first index i in the fundamental solution indicates the direction of the unit concentrated force at the source point \mathbf{x} . The Dirac δ function $\delta(\mathbf{x}, \mathbf{y})$ represents the body force corresponding to the unit concentrated force applied at \mathbf{x} .

Substituting Eqs. (9)–(11) into identity (8) and applying Eq. (2a), the following representation integral of the displacement field in domain Ω can be obtained:

$$\begin{aligned} \hat{u}_i(\mathbf{x}) &= \int_{\Gamma} U_{ij}(\mathbf{x}, \mathbf{y}) t_j(\mathbf{y}) d\Gamma - \int_{\Gamma} T_{ij}(\mathbf{x}, \mathbf{y}) \hat{u}_j(\mathbf{y}) d\Gamma + \int_{\Omega} V_{ij}(\mathbf{x}, \mathbf{y}) \hat{u}_j(\mathbf{y}) d\Omega \\ &\quad + \omega^2 \int_{\Omega} \frac{\rho(\mathbf{x})}{\mu} U_{ij}(\mathbf{x}, \mathbf{y}) \hat{u}_j(\mathbf{y}) d\Omega \end{aligned} \quad (12)$$

in which, traction $t_j = \sigma_{jk} n_k$, the first domain integral is due to the inhomogeneity of the material, and the second domain integral represents the inertial effect. The new kernel function V_{ij} is given by:

$$\begin{aligned} V_{ij} &\equiv \frac{\mu_{,k} \Sigma_{ijk}}{\mu} \\ &= \frac{-1}{4\pi(1-\nu)r} [(1-2\nu)(\hat{\mu}_i r_j - \hat{\mu}_j r_i) + ((1-2\nu)\delta_{ij} + 2r_i r_j) r_i \hat{\mu}_j]. \end{aligned} \quad (13)$$

And the normalized displacement and shear modulus are reformed as

$$\hat{u}_i(\mathbf{x}) = \kappa(\mathbf{x}) u_i(\mathbf{x}) \text{ and } \hat{\mu}(\mathbf{x}) = \ln \mu(\mathbf{x}). \quad (14a, b)$$

Once the displacement u_i and traction t_i are obtained on the entire

Table 1
Material properties of each component.

Materials	E (GPa)	ρ (kg/m ³)	ν
Steel (S)	200	7800	0.3
Aluminum (A)	70	2700	0.3

boundary Γ , the preceding integral expression can be used to evaluate the displacement at any point inside the domain Ω , if needed. Let the source point \mathbf{x} approach boundary Γ in Eq. (12), one obtains the following conventional BIE for the wave propagation problems in the FGM:

$$c_{ij}(\mathbf{x})\hat{u}_i(\mathbf{x}) = \int_{\Gamma} U_{ij}(\mathbf{x}, \mathbf{y})t_j(\mathbf{y})d\Gamma - \int_{\Gamma} T_{ij}(\mathbf{x}, \mathbf{y})\hat{u}_j(\mathbf{y})d\Gamma + \int_{\Omega} V_{ij}(\mathbf{x}, \mathbf{y})\hat{u}_j(\mathbf{y})d\Omega + \omega^2 \int_{\Omega} \frac{\rho(\mathbf{x})}{\kappa(\mathbf{x})} U_{ij}(\mathbf{x}, \mathbf{y})\hat{u}_j(\mathbf{y})d\Omega \quad (15)$$

where the coefficients $c_{ij} = 1/2\delta_{ij}$, if Γ is smooth at source point \mathbf{x} . Different method can be used to solve this conventional BIE for the dynamic FGM problem. In this work, the normalized displacements in the domain integrals in Eq. (15) are expressed by a combination of the fourth order spline-type radial basis function ϕ^A (Yang et al., 2014a; Gao et al., 2008) and the polynomials listed below with α_i^A , a_j^k and a_j^0 being the unknown coefficients:

$$\hat{u}_i(\mathbf{y}) = \sum_A \alpha_i^A \phi^A + a_i^k y_k + a_i^0, \quad \sum_A \alpha_i^A = 0, \quad \sum_A \alpha_i^A y_j^A = 0, \quad (16a, b, c)$$

where y_k and y_j^A are the coordinates of the field point \mathbf{y} and the

application point A respectively. The application points are composed by the boundary nodes and internal points. Substituting all the application points into Eq. (16), and if with no two coincide nodes, the unknow parameters can be calculated first (Yang et al., 2014b). Then, using the radial integral method (Gao, 2002), the domain integrals in Eq. (15) are transformed into boundary integrals as following and a BIE with only boundary integrals can be obtained.

$$\int_{\Omega} V_{ij}(\mathbf{x}, \mathbf{y})\hat{u}_j(\mathbf{y})d\Omega = \alpha_i^A \int_{\Gamma} \frac{1}{r} \frac{\partial r}{\partial n} \bar{V}_{ij} \int_0^r \phi^A dr d\Gamma + \frac{a_j^k}{2} \int_{\Gamma} r r_{,k} \frac{\partial r}{\partial n} \bar{V}_{ij} d\Gamma + (a_j^k x_k + a_j^0) \int_{\Gamma} \frac{\partial r}{\partial n} \bar{V}_{ij} d\Gamma, \quad (17)$$

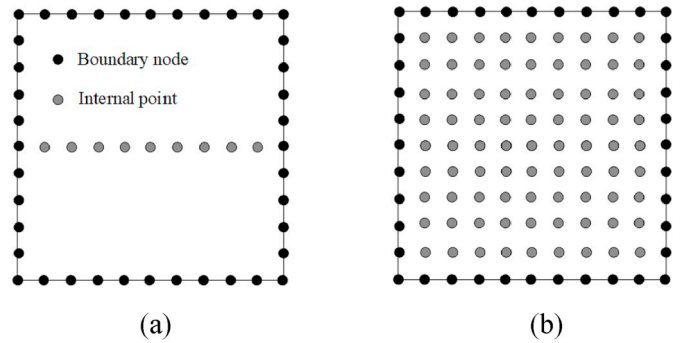


Fig. 4. BEM models with (a) 20 BE 9 IN (b) 20 BE 81 IN.

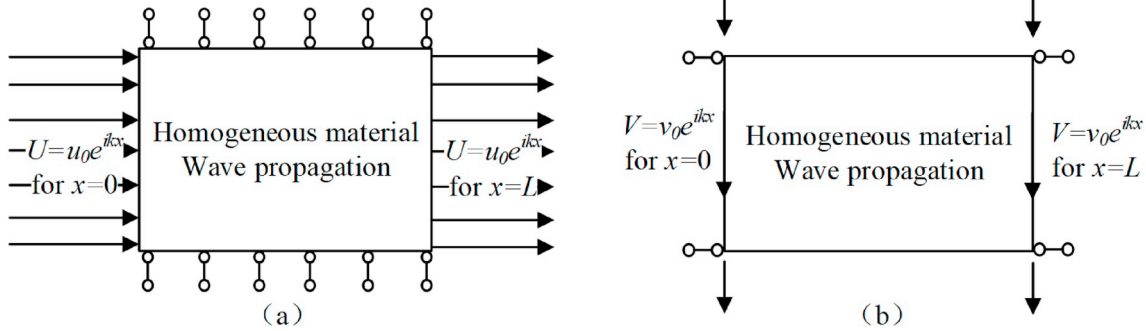


Fig. 2. Models of wave propagation in homogeneous media (a) P-wave (b) SV-wave.

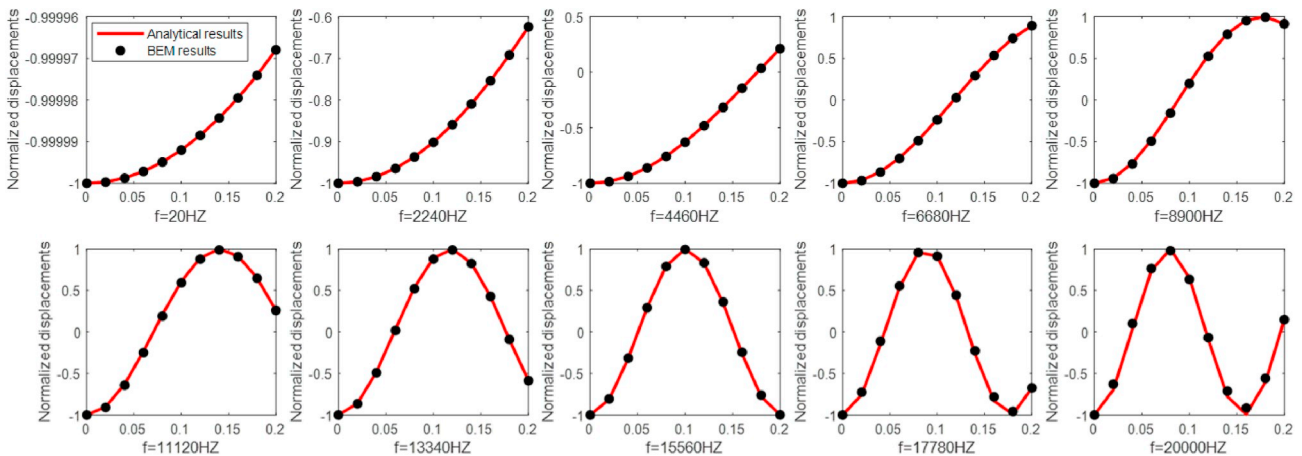
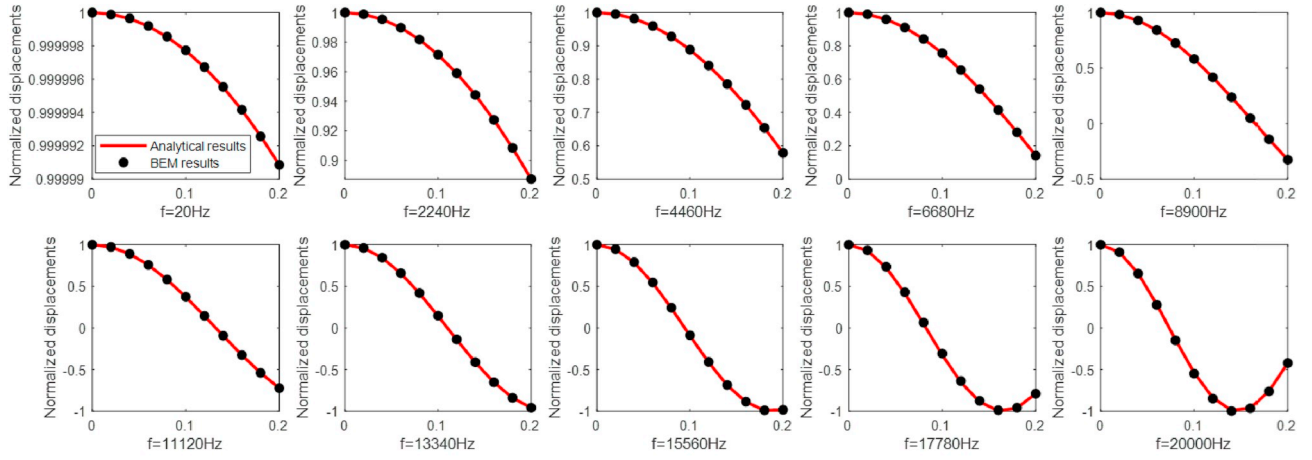
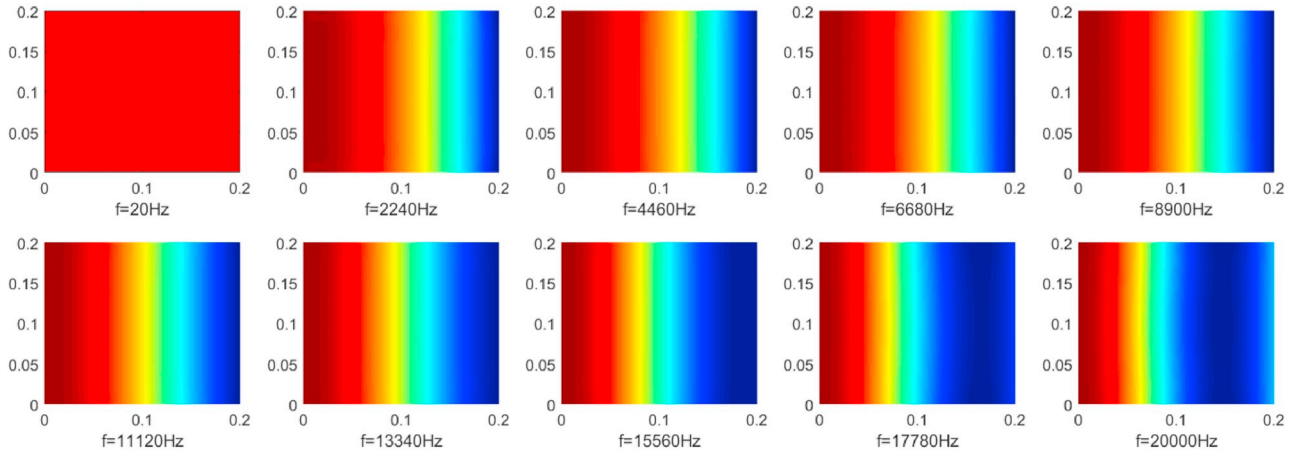


Fig. 3. The BEM results of SV-wave for homogeneous material compared with the analytical results.



(a)



(b)

Fig. 5. P-wave propagation in homogeneous material (a) Comparison normalized displacements with those of analytical solution; (b) displacement contour plots (20B81I).

$$\begin{aligned}
 \int_{\Omega} \frac{\rho(\mathbf{x})}{\kappa(\mathbf{x})} U_{ij}(\mathbf{x}, \mathbf{y}) \hat{u}_j(\mathbf{y}) d\Omega &= \frac{\rho_0}{\mu_0^2} \alpha_j^A \int_r^1 \frac{1}{r} \frac{\partial r}{\partial n} \int_0^r r \phi^A U_{ij} e^{i[(\xi-\beta)y_1 + (\eta-\gamma)y_2]} dr d\Gamma \\
 &+ a_j^k \int_r^1 \frac{r_k}{r} \frac{\partial r}{\partial n} \int_0^r r^2 U_{ij} e^{i[(\xi-\beta)y_1 + (\eta-\gamma)y_2]} dr d\Gamma \\
 &+ (a_j^k x_k + a_j^0) \int_r^1 \frac{1}{r} \frac{\partial r}{\partial n} \int_0^r r U_{ij} e^{i[(\xi-\beta)y_1 + (\eta-\gamma)y_2]} dr d\Gamma
 \end{aligned} \tag{18}$$

The BEM is applied to discretize this conventional BIE with quadratic boundary elements and internal nodes. The details of the implementation on calculating the boundary integrals can be found in Refs. (Yang et al., 2015, 2016). After substituting the boundary conditions, and the incident wave condition, the wave propagation displacement can be obtained by solving the linear equations shown below:

$$[\mathbf{A} - \omega^2 \mathbf{P}] \{\mathbf{z}\} = \{\mathbf{b}\}, \tag{19}$$

where \mathbf{A} and \mathbf{P} are coefficient matrices, \mathbf{z} vector contains all the unknown displacements and tractions at each node, and \mathbf{b} is the known right-hand-side vector. By solving Eq. (19), all the unknown boundary variables on each element can be obtained.

4. Numerical examples

A steel/aluminum FGM is considered in this study, the material properties of each components are listed in Table 1.

For all the analyses, the waves are introduced due to a harmonic initial displacement as $U(x) = u_0 e^{ikx}$ (x-direction) or $V(x) = v_0 e^{ikx}$ (y-direction). After solution, the obtained displacements are all normalized as:

$$\bar{u}(x) = u / u_0 \text{ or } \bar{v}(x) = v / v_0. \tag{20}$$

4.1. Verification of the present method

4.1.1. Verification of the wave propagation in homogeneous materials

The present method is first verified by analyzing the P-wave and SV-wave propagation in the homogenous media, and the models are depicted in Fig. 2. The length of each side of this domain is 0.2 m.

It is found that the BEM solution with only 20 quadratic boundary elements (BE) and 9 internal nodes (IN) can already yield accurate results compared with the analytical results with the form of $u(x) = u_0 e^{ikx}$, where u_0 is the constant coefficient of amplitude, k is the incident wave number and $i = \sqrt{-1}$ is the imaginary unit. For the incident wave frequency ranging from 20 Hz to 20000 Hz, comparisons of the BEM and

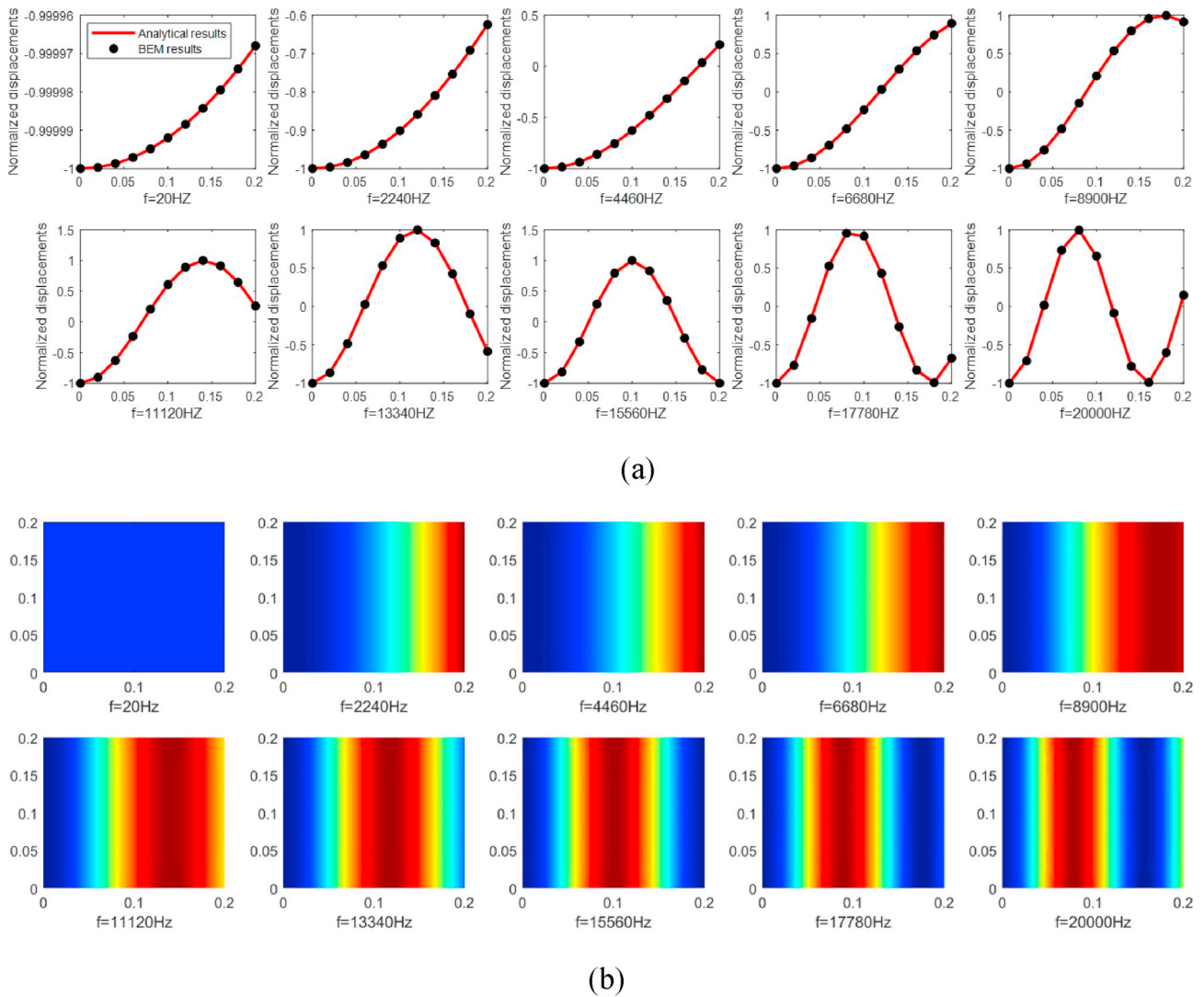


Fig. 6. SV-wave propagation in homogeneous material (a) Comparison normalized displacements with those of analytical solution; (b) displacement contour plots (20B81I).

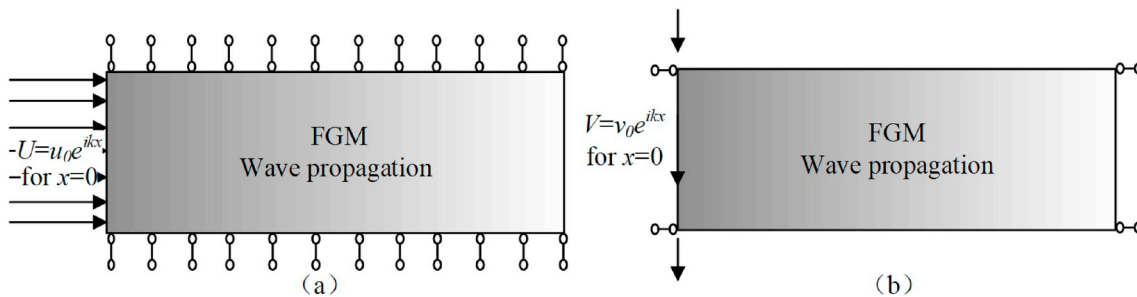


Fig. 7. Models of the P- and SV- wave propagation in FGM.

analytical displacements are shown in Fig. 3, with the corresponding BEM model shown in Fig. 4 (a).

Increasing the internal nodes can increase the accuracy of the results. The model with 20 boundary elements and 81 internal nodes (Fig. 4(b)) is used to calculate the normalized displacements of P-wave and SV-wave in the homogeneous material case, with the incident wave frequency ranging from 20 Hz to 20000 Hz. The BEM normalized displacements are compared with the analytical solution and their displacements contours are plotted in Figs. 5 and 6. It can be seen that

the BEM results with 20 boundary elements and 81 internal nodes match well with those of the exact solutions. It can be concluded that, the BEM developed is effective and accurate in the homogeneous material case.

4.1.2. Verification of the wave propagation in FGM

Due to the frequency domain wave propagation in FGM is very limited in literature, the present results of frequency wave propagation in the FGM is compared with that of the finite element method (FEM), which is calculated by applying the commercial software ABAQUS. The

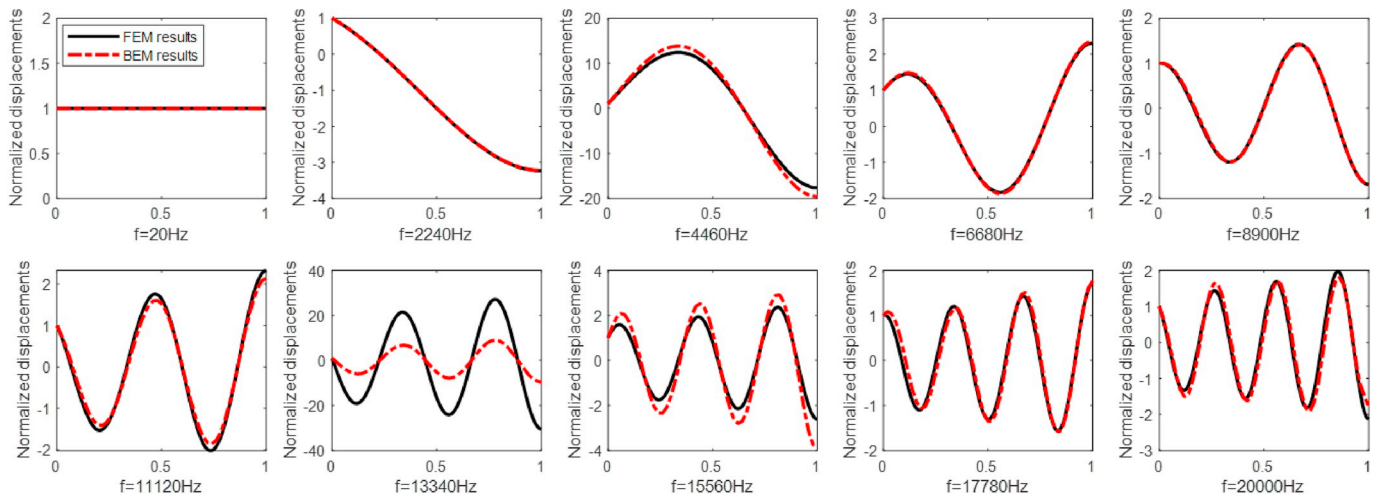


Fig. 8. Comparison of the normalized displacements of P-wave in SAX1 FGM with those of the FEM.

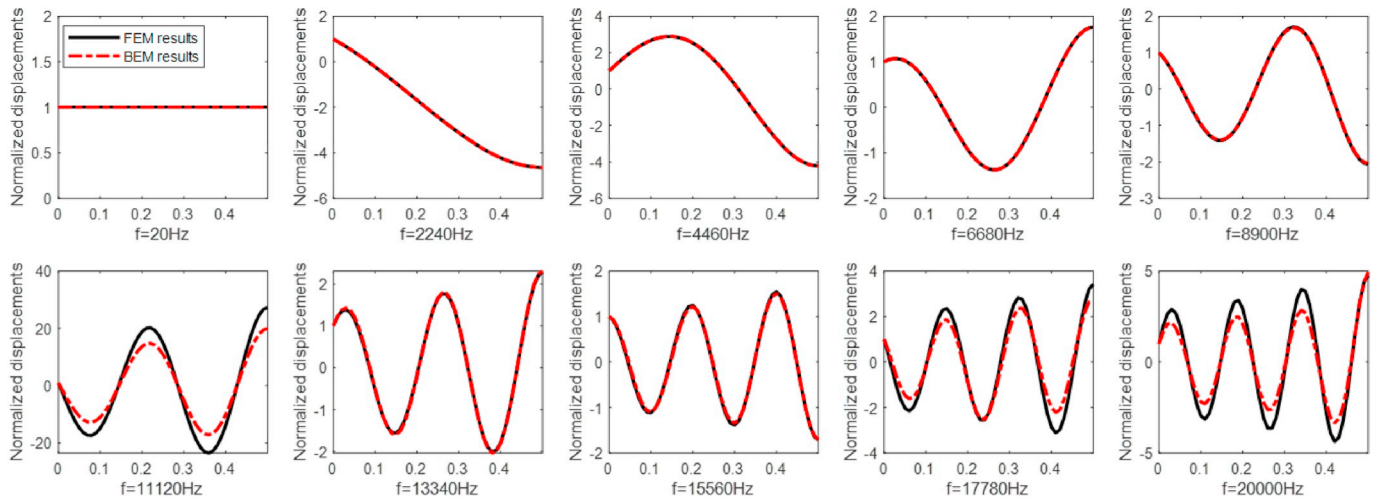


Fig. 9. Comparison of the normalized displacements of SV-wave in SAX1 FGM with those of the FEM.



Fig. 10. Six cases of FGM models.

model of the P- and SV-wave propagation is given in Fig. 7. The lengths of the considered rectangular domain of P- and SV-wave are 1 m and 0.5 m, and the heights are all 0.2 m. In this stage, only one FGM case is used to verification. That is the materials of the FGM vary continuously from steel to aluminum in x_1 direction, and which is named SAX1.

The normalized displacements of the P-wave propagation in SAX1 FGM computed by present BEM using 60 BE 273 IN and FEM using 2000 quadratic elements are plotted in Fig. 8. It can be seen that, the BEM and FEM results matched well, except for the cases with $f=13340$ Hz. That is because when the incident wave frequency is $f=13340$ Hz, a

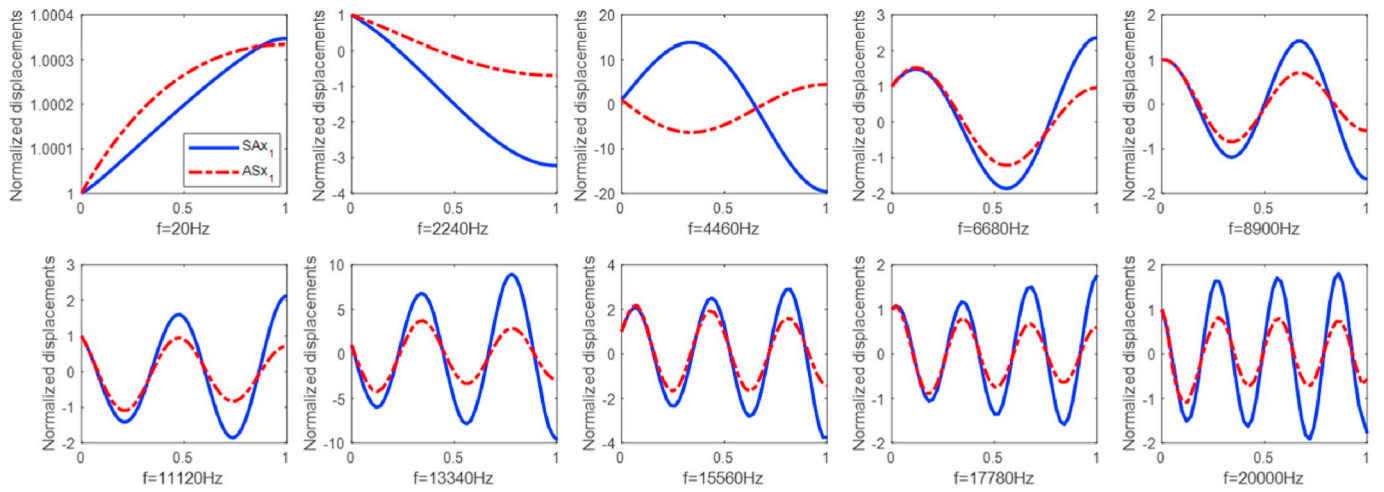


Fig. 11. Normalized displacement of P-wave propagation in SAX_1 and ASX_1 FGM.

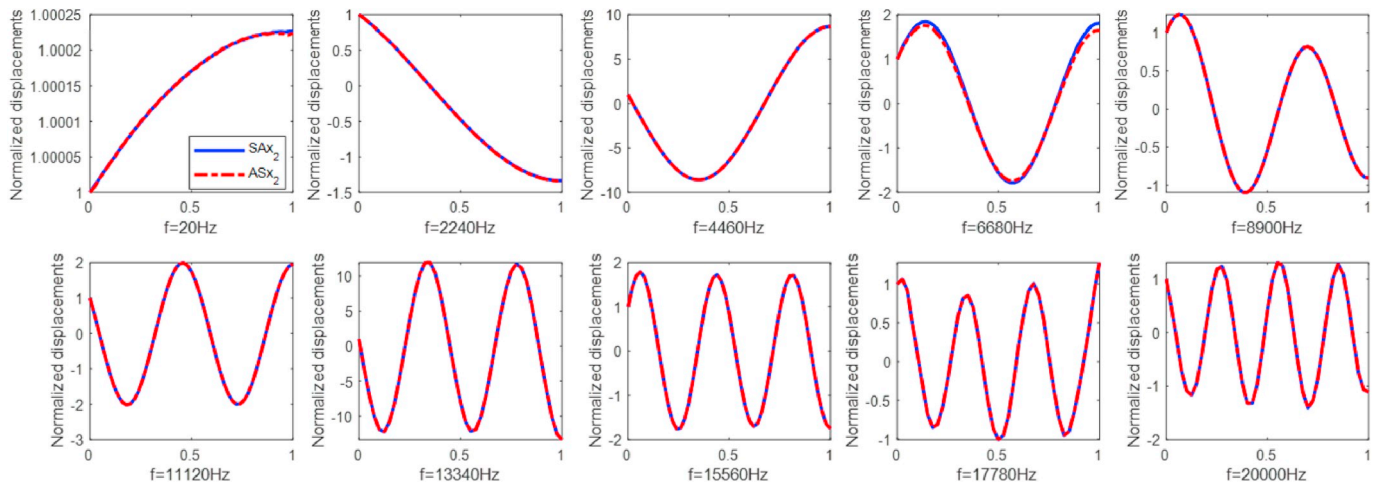


Fig. 12. Normalized displacement of P-wave propagation in SAX_2 and ASX_2 FGM.

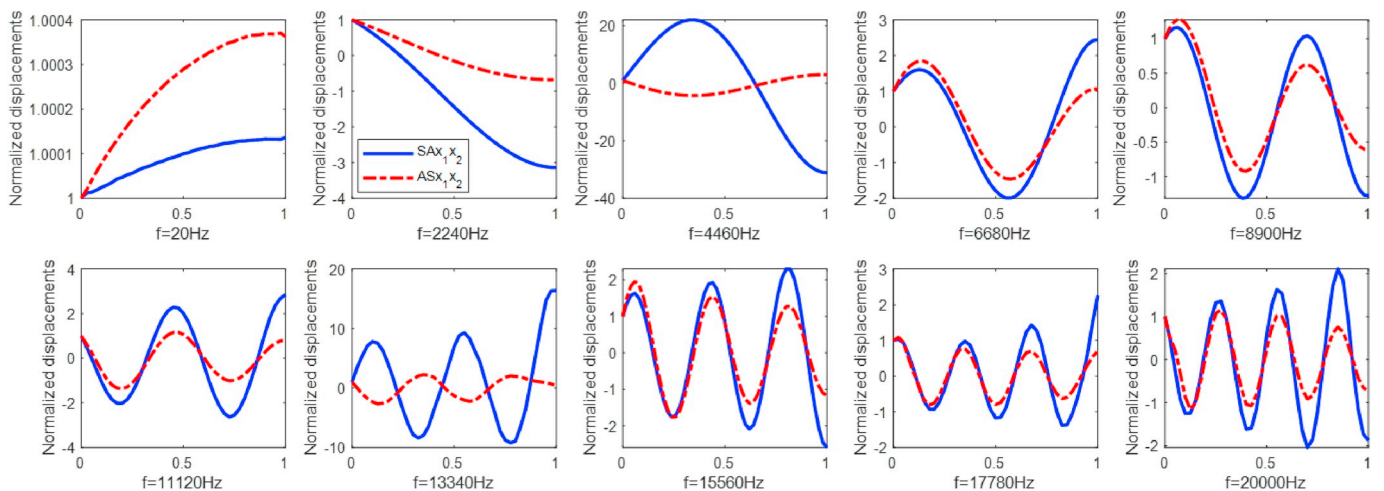


Fig. 13. Normalized displacement of P wave propagation in SAX_1x_2 and ASX_1x_2 FGM.

resonance of this considered structure is occurred. The displacements calculated by the FEM is almost two times of that of the present BEM at this frequency.

The normalized displacements of the SV-wave propagation in SAX_1

FGM computed by the BEM using 70 BE 147 IN and the FEM using 1000 quadratic elements are plotted in Fig. 9. A structural resonance is also occurred in $f = 11120$ Hz. It can be shown that the results are compared very well at all frequencies in this case.

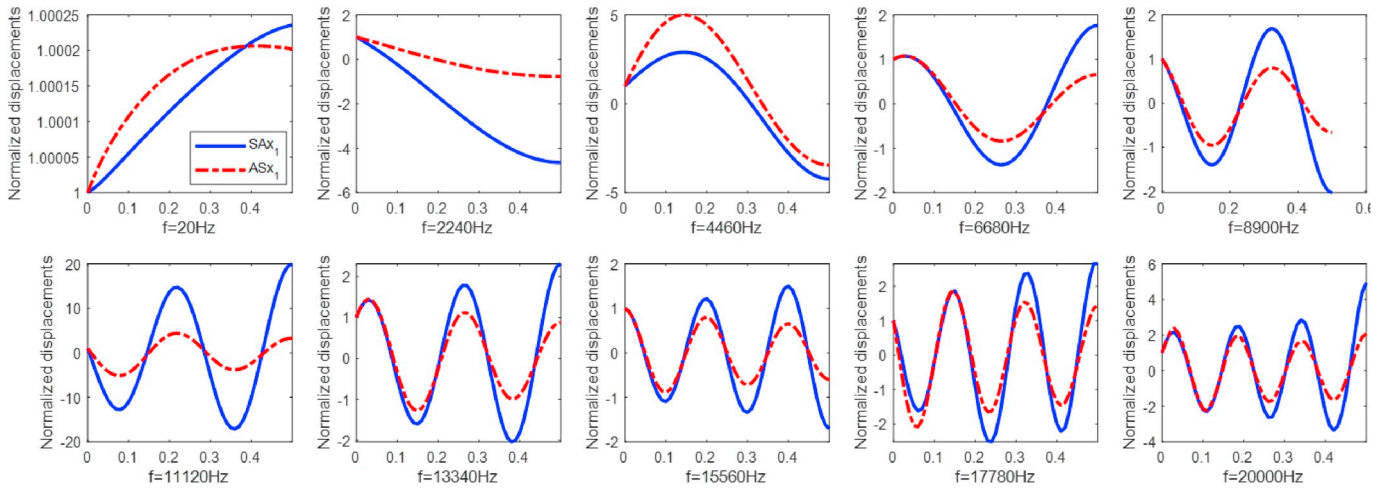


Fig. 14. Normalized displacements of SV-wave propagation in SAX_1 and ASX_1 FGMs.

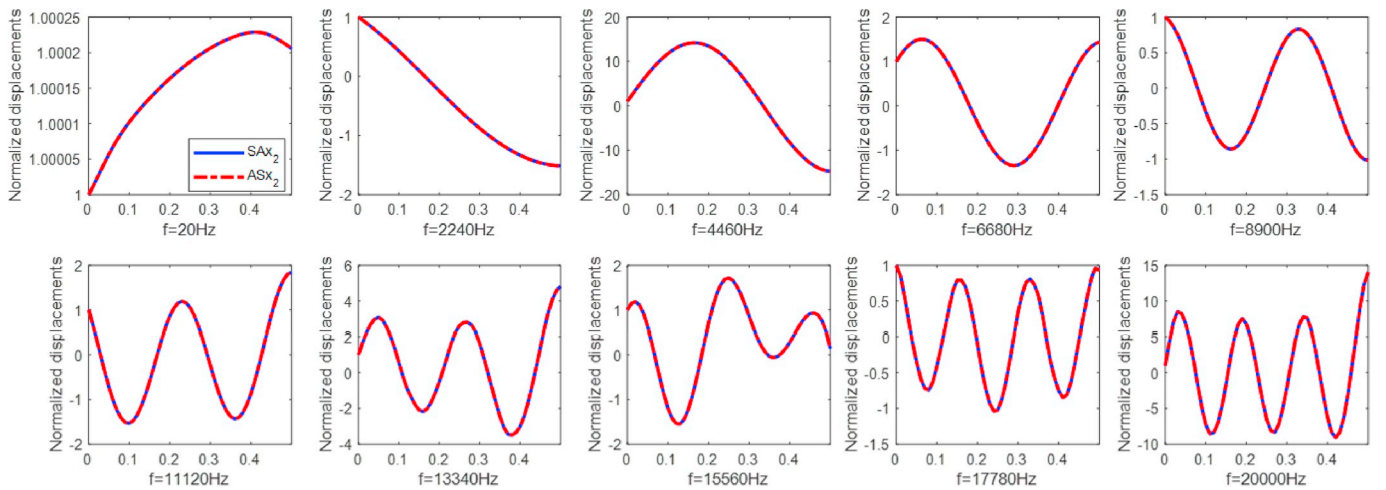


Fig. 15. Normalized displacement of SV-wave propagation in SAX_2 and ASX_2 FGMs.

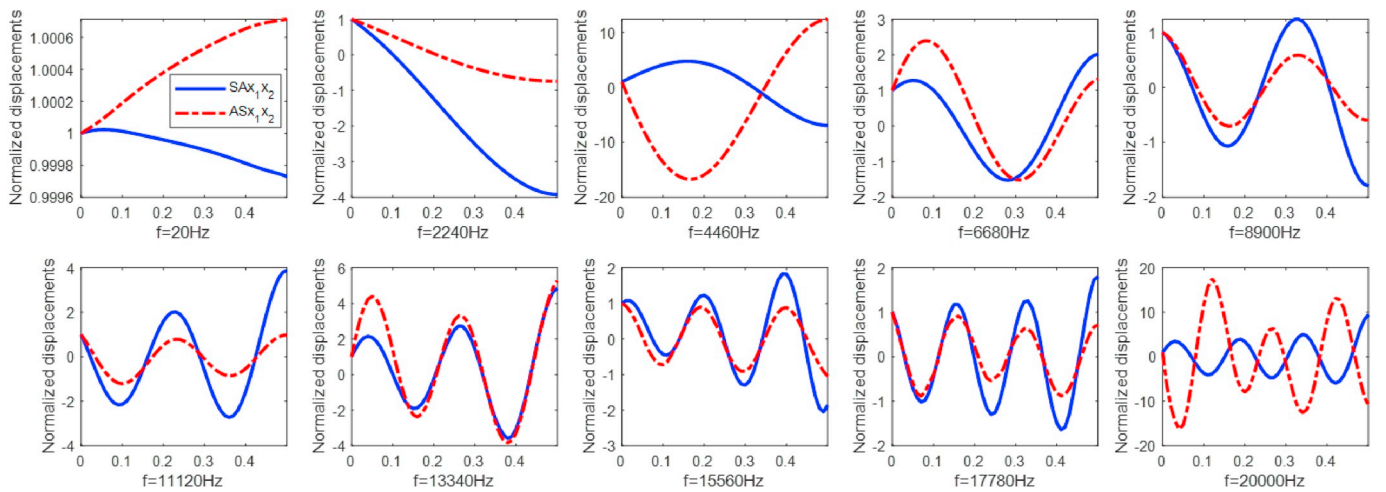


Fig. 16. Normalized displacement of SV-wave propagation in SAX_1x_2 and ASX_1x_2 FGMs.

4.2. Wave propagation in the FGM media

In this section, the P-wave and SV-wave propagation in the FGM media is further investigated. Three different cases of different material

gradation directions and two different material gradients are considered. Namely, material gradation only in x_1 direction, or only in x_2 direction, or in x_1 and x_2 directions simultaneously; meanwhile, the material graduates from steel to aluminum or from aluminum to steel;

with a total number of six cases. For convenience, SAX_1 is used to denote the case that material properties gradate from steel to aluminum in x_1 direction, and the same way to define SAX_2 , SAX_1x_2 , ASX_1 , ASX_2 and ASX_1x_2 (Fig. 10).

4.2.1. P-wave propagation

The considered model of P-wave propagating in FGM is described in this subsection and their results are presented in Figs. 11–13.

Six cases of P-wave propagation in FGM are investigated. SAX_1 and ASX_1 wave propagation are presented in Fig. 11. For these two cases of P-wave propagation, the propagation direction is the same as the material gradation direction, and a phenomenon that the amplitude varies with the frequency is emerged. With decreasing material stiffness, the amplitudes are amplified; and inverse, stiffening the material properties, the amplitudes are attenuated. Meanwhile, the amplitude of variation is enhanced with the incident wave frequency increased. If the material gradient is normal to the wave propagation, less effect of the material gradient on the variation of the wave amplitude, which can be observed in Fig. 12, where SAX_2 and ASX_2 waves are plotted and they are almost the same. Material gradation in x_1x_2 are depicted in Fig. 13, where the material gradients affect the wave propagation much more. With high incident wave frequency, the amplitude variations are much more obviously, and the trend of variation is the same as that in the SAX_1 and ASX_1 cases.

4.2.2. SV-wave propagation

The SV-wave propagating in FGM model is described and the normalized displacements of the considered six cases of FGMs are plotted in Figs. 14–16.

From Fig. 14, it can be seen that, although the nodes vibrate normal to the wave propagation direction, the wave propagation is in accordance with the material gradation, which still leads to the variation of the wave amplitudes. With the increase of the incident wave frequency, the SAX_1 wave amplitudes increase, while the ASX_1 wave attenuations amplify.

When the node vibration direction is in accordance with the material gradation direction, or the SV-wave propagation is normal to the material gradation direction. It is observed from Fig. 15 that the wave displacements of SAX_2 and ASX_2 are the same, the amplitudes of the waves are not changed with the material gradation. From this result, it may be concluded that when the material gradients normal to the wave propagation direction, it will have less effect on the wave propagation.

Finally, cases of the material gradating simultaneously in x_1 and x_2 are considered for the SV-wave. There is still some variation of the material properties in the wave propagation direction, thus changes of the wave amplitudes of SAX_1x_2 and ASX_1x_2 are observed. Excepted for the resonant frequencies, the variation of the wave amplitude is almost relating to the variation of the material properties.

From the above analyses of the wave propagation in FGM models, it can be concluded that whenever for P- or SV-wave, only two different cases should be considered: 1) when the wave propagates in the direction of gradation; and 2) when the propagation is in the direction normal to the gradation direction. The first case gives rise to an inhomogeneous wave, where the wave amplitude varies while propagating, for which stiffening the material properties decreases the amplitude and decreasing the material stiffness increases the wave amplitude. This phenomenon is missing in the second case, which will be refer to as the homogeneous wave case.

5. Conclusions

A new boundary element method for modeling wave propagation in

FGMs is proposed and verified using several 2-D FGM models. In this paper, there are three novelties as listed below: First, a generalized Green's identity corresponding to the elastodynamic equations for FGMs is established by using the Gauss theorem. This new derived Green's identity can be applied to solve elastodynamic problems of FGMs for either 2-D or 3-D models. Second, based on this Green's identity, the BIE for FGM elastodynamic equations is derived analytically, which can be used to distinguish the BIE derived by using the weighted residual method. The last but not least, the present developed approach is used to model the wave propagation problems in FGM.

The verification of the present BEM results with that of the analytical solution demonstrates that the BEM can provide numerical results with high efficiency and accuracy. A parametric study is conducted to investigate the effects of the material gradients, gradation direction, as well as incident wave frequencies on the wave propagation in the FGMs. It is concluded that, the amplitude of inhomogeneous wave varies while propagating and this phenomenon is missing in the homogeneous wave case. Increasing the stiffness of the materials can attenuate the waves and decreasing the stiffness of the materials can amplify the waves. The present BIE formulation can be used as the theoretical basis for the analysis of wave propagation in FGMs using both 2-D and 3-D models, and it also can be applied to analyze other elastodynamic FGM problems, such as structure dynamic analysis.

Acknowledgement

The authors gratefully acknowledge the National Natural Science Foundation of China for financial support to this work under Grant NSFC no. 11901283.

References

- Aksoy, H.G., Senocak, E., 2009. Wave propagation in functionally graded and layered materials. *Finite Elem. Anal. Des.* 45 (12), 876–891.
- Aminipour, H., Janghorban, M., Li, L., 2018. A new model for wave propagation in functionally graded anisotropic doubly-curved shells. *Compos. Struct.* 190, 91–111.
- Bednarik, M., Cervenka, M., Groby, J.P., et al., 2018. One-dimensional propagation of longitudinal elastic waves through functionally graded materials. *Int. J. Solids Struct.* 146, 43–54.
- Berezovski, A., Engelbrecht, J., Maugin, G.A., 2003. Numerical simulation of two-dimensional wave propagation in functionally graded materials. *Eur. J. Mech. A Solid.* 22 (2), 257–265.
- Bruck, H.A., 2000. A one-dimensional model for designing functionally graded materials to manage stress waves. *Int. J. Solids Struct.* 37 (44), 6383–6395.
- Chakraborty, A., Gopalakrishnan, S., 2004. A higher-order spectral element for wave propagation analysis in functionally graded materials. *Acta Mech.* 172 (1–2), 17–43.
- Dorduncu, M., Apalak, M.K., Reddy, J., 2019. Stress wave propagation in adhesively bonded functionally graded cylinders: an improved model. *J. Adhes. Sci. Technol.* 33 (2), 156–186.
- Dorduncu, M., Kemal Apalak, M., Cherukuri, H.P., 2015. Elastic wave propagation in functionally graded circular cylinders. *Compos. Part B Eng.* 73, 35–48.
- Fengxiang, X., Xiong, Z., Hui, Z., 2018. A review on functionally graded structures and materials for energy absorption. *Eng. Struct.* 171, 309–325.
- Fourn, H., Atmane, H.A., et al., 2018. A novel four variable refined plate theory for wave propagation in functionally graded material plates. *Steel Compos. Struct.* 27, 109–122.
- Gao, X.W.A., 2002. Boundary element method without internal cells for two-dimensional and three-dimensional elastoplastic problems. *J. Appl. Mech.* 69 (2), 154.
- Gao, X.W., Davies, T.G., 2011. *Boundary Element Programming in Mechanics*.
- Gao, X.W., Zhang, Ch., Sladek, J., Sladek, V., 2008. Fracture analysis of functionally graded materials by a BEM. *Compos. Sci. Technol.* 68, 1209–1215.
- Gopalakrishnan, S., 2016. *Wave Propagation in Materials and Structures*. CRC Press.
- Hedayatrasa, S., Bui, T.Q., Zhang, C., et al., 2014. Numerical modeling of wave propagation in functionally graded materials using time-domain spectral Chebyshev elements. *J. Comput. Phys.* 258, 381–404.
- Liu, Y.J., 2009. *Fast Multipole Boundary Element Method - Theory and Applications in Engineering*. Cambridge University Press, Cambridge.
- Mahamood, R.M., Akinlabi, E.T., 2017. *Types of Functionally Graded Materials and Their Areas of Application*. Springer International Publishing.

- Sun, D., Luo, S.N., 2011. The wave propagation and dynamic response of rectangular functionally graded material plates with completed clamped supports under impulse load. *Eur. J. Mech. A Solid*. 30 (3), 396–408.
- Yang, Y., Kou, K.P., Iu, V.P., Lam, C.C., Zhang, C.Z., 2014a. Free vibration analysis of two-dimensional functionally graded structures by a meshfree boundary-domain integral equation method. *Compos. Struct.* 110, 342–353.
- Yang, Y., Lam, C.C., Kou, K.P., Iu, V.P., 2014b. Free vibration analysis of the functionally graded sandwich beams by a meshfree boundary-domain integral equation method. *Compos. Struct.* 117, 32–39.
- Yang, Y., Lam, C.C., Kou, K.P., Iu, V.P., 2015. Free vibration analysis of two-dimensional functionally graded coated and undercoated substrate structures. *Eng. Anal. Bound. Elem.* 60, 10–17.
- Yang, Y., Lam, C.C., Kou, K.P., 2016. Forced vibration analysis of functionally graded beams by the meshfree boundary-domain integral equation method. *Eng. Anal. Bound. Elem.* 72, 100–110.